Design of Multi-Sensor Attitude Determination Systems

DEMOZ GEBRE-EGZIABHER
University of Minnesota, Twin Cities

ROGER C. HAYWARD
GeoTrax Protection, LLC

J. DAVID POWELL
Stanford University

The design of inexpensive multi-sensor attitude determination systems is discussed. The systems discussed fuse information from a triad of solid state rate gyros with an aiding system mechanized using GPS or magnetometers and accelerometers. Euler angle and quaternion-based sensor fusion algorithms are developed. Methods for gain scheduling and estimator pole placement are presented. Using simulation and flight test results, it is shown that quaternion-based algorithms simplify gain scheduling and improve transient response.

Manuscript received July 24, 2003; released for publication March 8, 2004.

IEEE Log No. T-AES/40/2/831384.

Refereeing of this contribution was handled by M. Kayton.

This work was sponsored by a research grant from the Federal Aviation Administration Satellite Program Office and a NASA-Langley technology transfer grant from Seagull Technology Inc.

Authors' addresses: D. Gebre-Egziabher, Dept. of Aerospace Engineering and Mechanics, University of Minnesota, Twin Cities Campus, 110 Union St. S.E., Minneapolis, MN 55455; R. C. Hayward, GeoTrax Protection, LLC, 16611 E. Laser Drive, Fountain Hills, AZ 85268; J. D. Powell, Professor Emeritus, Dept. of Aeronautics and Astronautics, Stanford University, Stanford, CA.

I. INTRODUCTION

Attitude is the term used to describe a vehicle's orientation in space and an attitude heading reference system (AHRS) is a device used to determine a vehicle's attitude. The attitude information generated by an AHRS is used in many navigation, guidance, and control applications such as pilot-in-the-loop control of manned aircraft. Devices such as automatic pilots also use the attitude information generated by an AHRS. Until recently, cost-sensitive applications such as uninhabited aerial vehicles (UAV) and general aviation mostly relied on AHRS that use mechanical gyros (similar to the one described in [1]) as the primary sensor. The mechanical gyros for indicating pitch and roll attitude consist of a spinning rotor mounted on a two axis gimbal. A separate rotor is used for heading. The aircraft's vacuum or electrical system provides the power needed to spin the gyro rotors. One drawback of these mechanical gyros is that they have too many moving parts and, thus, lack reliability.

In the past decade, gyros based on solid-state sensor technology have become readily available and have supplanted mechanical gyros in some aerospace applications. Unlike mechanical gyros, these solid-state sensors do not rely on numerous and large moving parts. Instead, they use miniature sensing elements made from quartz crystals [2] or micro-machined silicon [3]. In some cases, they use optical sensing elements in the form of a fiber-optic coil [4] or a glass resonant cavity [5]. Thus, these gyros are normally smaller in size and weight than mechanical gyros. They also consume less power and tend to be more reliable. Such features make solid-state gyros an attractive alternative because reliability, size, weight, and power consumption are important design constraints in many aerospace applications.

Successful implementation of an AHRS requires the use of rate gyros with exceptionally accurate and stable outputs (i.e., output errors less than 0.1°/h). Even though such highly accurate solid-state rate gyros are available, they can be relatively expensive and, therefore, not practical for use in most UAV and general aviation applications. While inexpensive ($< \$1000$ per axis) solid-state rate gyros are available, they tend to be low-performance sensors. That is, they have outputs subject to wideband noise and rate instabilities on the order of 10 to 100°/h. The attitude solution generated using these gyros is, therefore, prone to unbounded, bias, and random-walk errors. An AHRS can be successfully implemented using inexpensive rate gyros provided there is a means for aiding the rate gyros or resetting the attitude errors periodically.

There has been some effort directed at developing inexpensive, gyro-free attitude determination systems

that can be used to aid rate gyros. This effort has been facilitated by the availability of other inexpensive solid state sensors such as magnetometers, accelerometers and air data systems. Position and attitude sensors like the Global Positioning System (GPS) are also being used. For example, [6] discusses an inexpensive attitude determination system for aviation applications. This attitude determination system does not use rate gyros. Instead, it relies on a kinematic model of the vehicle along with GPS measurements of position and velocity. These measurements are used to generate what is called "pseudoattitude." Another inexpensive gyro-free attitude determination system is presented in [7]. The system presented in [7] uses magnetometers, accelerometers, and GPS as the primary sensors and determines attitude by solving Wahba's problem [8]. A potentially inexpensive, gyro-free multi-antenna GPS-based attitude determination system is discussed in [9] and [10]. This system uses carrier phase differential GPS techniques to determine the relative orientation of three or more GPS antennas installed on a vehicle. Vehicle attitude can be deduced from knowledge of the antennas' relative orientation in space.

In many practical applications, these gyro-free systems cannot be used alone. There are several reasons for this. Firstly, these gyro-free systems are generally not capable of providing high-bandwidth attitude information. Secondly, they cannot generate a valid attitude solution during certain vehicle maneuvers. For example, the GPS attitude determination system cannot generate a valid attitude information during maneuvers where the line of sights between the GPS antennas and satellites are blocked (e.g., inverted flight). Lastly, while the attitude solution generated by theses systems is normally drift-free, it can be relatively noisy due to wideband noise.

Inexpensive rate gyros can be used to generate a high bandwidth albeit biased attitude solution. Thus, sensor fusion techniques can be employed in such a way that the gyro-free systems are used to bound the rate gyro drift errors. The rate gyros, in turn, are used to "smooth" the aiding system's attitude solution. The tool used for blending the complementary characteristics of the rate gyros and the gyro-free aiding systems is an estimator. This sensor fusion concept is shown schematically in Fig. 1. Even though this figure is discussed in greater detail later in the paper, at this point is only important to note the overall architecture of the system. The AHRS depicted is a multi-sensor system that combines low-performance rate gyros with an aiding system. It exploits the complementary nature of the rate gyros and the aiding systems to generate a high-bandwidth, drift-free attitude solution.

The purpose of this paper is to describe the design and analyze the performance of estimators

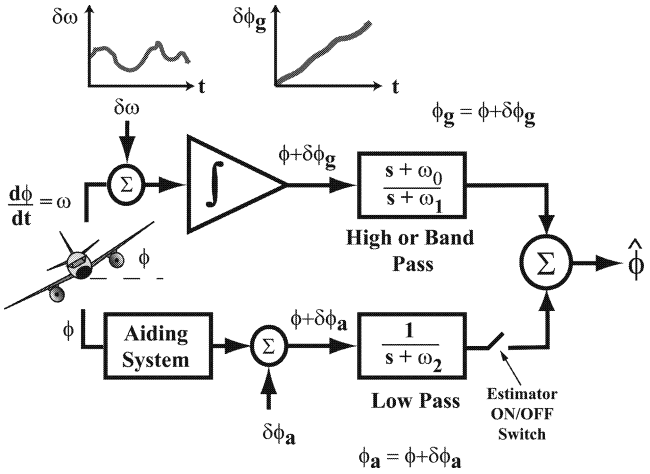

Fig. 1. Sensor fusion based attitude determination system. ϕ_g is attitude solution generated by rate gyros while ϕ_a is aiding system's attitude solution.

(complementary filters) used to mechanize a multi-sensor AHRS as shown in Fig. 1. The idea of blending rate gyros and an aiding system's information using a complementary filter is not new. Such methods have been used in satellite attitude determination systems for decades. For example, [11] discusses a satellite attitude determination system that fuses rate gyros with star trackers. The estimator used in [11] is based on earlier work described in [12] and [13]. The systems described here, however, are different from the ones considered in [11], [12], and [13] because they use considerably less accurate sensors. Furthermore, the microprocessors used to execute the sensor fusion algorithms in real-time may have limited computational power. The use of such sensors and microprocessors has an impact on the overall estimator architecture. It affects issues such as pole placement (or estimator tuning) and gain scheduling.

Accordingly, the remainder of this paper is organized as follows. In Section II, the basics of attitude determination using rate gyros is discussed. This discussion includes a description of a unified rate gyro error model developed for this work. Experimentally derived values for the error model parameters of various inexpensive rate gyros are also presented. It is quantitatively shown how these gyro errors (in the absence of an aiding system) lead to unbounded attitude errors. In Section III, methods for aiding rate gyros and bounding attitude errors is discussed. Section IV presents a qualitative overview of the estimators (Kalman filters) for fusing rate gyro information with an aiding system. In Section V, algorithmic details for mechanizing the multi-sensor AHRS are presented. Section VI presents quantitative results showing the advantages of fusing rate gyros with an aiding system. Section VII discusses estimator tuning and pole placement. In Section VIII, gain

scheduling issues are discussed. Section IX presents experimental flight test results for a multi-sensor AHRS. Section X concludes the paper.

II. OPEN-LOOP PERFORMANCE

An AHRS that relies on rate gyros as the only set of sensors will normally have an orthogonal triad of them affixed to the body of the vehicle. The rate gyros' sensitive axes will be aligned with each of the body axes of the vehicle. The angular rate measurements from the gyro triad are then used to solve a set of kinematic differential equations describing the vehicle's attitude. The form of these kinematic differential equations depends on the attitude description (parameterization) used. While there are numerous ways of parameterizing attitude, only Euler angles and quaternions are considered here. Even though Euler angles suffer from a singularity, we consider them here because they are somewhat intuitive and, thus, convenient for presenting performance analysis results. Furthermore, many AHRSs used for pilot-in-the-loop control display attitude in terms of Euler angles because they operate in a region where the Euler angle singularity is not an issue. Therefore, in these applications, it would be interesting to know if there are still other disadvantages to using the Euler angle representation of attitude. As shown later, when compared quaternion-based estimators, Euler angle estimators have some advantages as well as disadvantages.

If Euler angles are being used, the system of differential equations describing the vehicle's attitude are

$$\begin{bmatrix} \dot{\psi} \\ \dot{\theta} \\ \dot{\phi} \end{bmatrix} = \frac{1}{c_\theta} \begin{bmatrix} 0 & s_\phi & c_\phi \\ 0 & c_\phi c_\theta & -s_\phi c_\theta \\ c_\theta & s_\phi s_\theta & c_\phi s_\theta \end{bmatrix} \begin{bmatrix} p \\ q \\ r \end{bmatrix}. \tag{1}$$

The variables ψ, θ, and ϕ represent yaw, pitch, and roll, respectively. The variables s_ϕ, s_θ, c_ϕ, and c_θ are being used as compact notations for the trigonometric functions $\sin(\phi)$, $\sin(\theta)$, $\cos(\phi)$ and $\cos(\theta)$, respectively. The variables p, q, and r represent the angular rate measurements obtained from the three orthogonal rate gyros. More specifically, p is the output of the rate gyro with its sensing axis aligned with the roll axis. Similarly, q is the pitch axis rate gyro output and r is the yaw axis gyro output.

When attitude is parameterized using quaternions, the system of differential equations for the vehicle's attitude becomes

$$\dot{\mathbf{q}} = \tfrac{1}{2}\Omega \begin{bmatrix} q_0 \\ \vec{q}_v \end{bmatrix}. \tag{2}$$

The attitude quaternion $\mathbf{q}$ is equal to $[q_0 \ \vec{q}_v]^T$ where the scalar (q_0) and vector ($\vec{q}_v$) parts of $\mathbf{q}$ are defined as follows:

$$q_0 = \cos(\Phi) \tag{3}$$

$$\vec{q}_v = \sin(\Phi)\hat{e} = \begin{bmatrix} q_1 \\ q_2 \\ q_3 \end{bmatrix}. \tag{4}$$

The variables Φ and $\hat{e}$ come from Euler's rotation theorem. The theorem states that the orientation of one coordinate frame with respect to another, after a series of rotations, can be described by a single rotation of magnitude Φ about a single axis whose orientation in space is defined by the unit vector $\hat{e}$. Loosely, the first element of a quaternion describes the amount of rotation about the axis defined in the Euler rotation theorem. The vector part of the quaternion describes the orientation of the angle of rotation. A more precise mathematical definition and detailed treatment of attitude quaternions can be found in specialized books such as [14] or most advanced dynamics texts. The matrix Ω in (2) is given by

$$\Omega = \begin{bmatrix} 0 & -p & -q & -r \\ p & 0 & r & -q \\ q & -r & 0 & p \\ r & q & -p & 0 \end{bmatrix}. \tag{5}$$

Inspection of (1)–(5) shows that any angular rate measurement error will lead to attitude errors that grow with time. To better understand the nature of these unbounded attitude errors consider a case where the angular rate output from the roll axis gyro in error by an amount b_p. That is, the measured rate gyro output p_m is equal to the true angular rate p_t corrupted by a constant error b_p as shown below:

$$p_m = p_t + b_p. \tag{6}$$

In general, the output errors for low-performance rate gyros tend be stochastic in nature and not constant as shown in (6). Higher fidelity error models will be presented shortly but at this point it is sufficient to note that the designer of an AHRS has access only to the erroneous measurement p_m. Thus, when the expression for p_m is used in (1) (in lieu of p), it is clear to see that the angular rate measurement error b_p leads to a roll angle error $\delta\phi$. If the vehicle is level ($\theta = \phi = 0$), the rate at which the roll error grows, $\delta\dot{\phi}$, is equal to the angular rate measurement error b_p. Since the attitude differential equations are coupled, the roll error will eventually lead to pitch and yaw errors as well.

A. Rate Gyro Error Models

In order to perform a more realistic error analysis, higher fidelity gyro error models are required. This is because a realistic error or covariance analysis must account for both deterministic and stochastic gyro

errors. The covariance analysis that is subsequently discussed uses one such model that was developed in [15]. This error model is given by the following:

$$p_m = (1 + s_f)p_t + b_p(t). \tag{7}$$

In (7), p_m is the sensor's measured output. p_t is the true value of the angular rate that the rate gyro is attempting to measure. This true value is corrupted by a scale factor error s_f and a bias $b_q(t)$. This expression is equally applicable to the q and r angular measurements as well.

For clarity, we drop the subscript p from $b(t)$ for the moment. The bias term $b(t)$ has the following general form:

$$b(t) = b_0 + b_1(t) + b_w(t). \tag{8}$$

The term b_0 represents a constant null-shift. The remaining two terms, $b_1(t)$ and $b_w(t)$, are output errors which are stochastic in nature. The term $b_1(t)$ represents a time-varying component of the bias. The term $b_w(t)$ represents the sampling noise.

For most gyros, $b_1(t)$ can be accurately modeled as an exponentially correlated Gaussian random process with a variance $\sigma_{b_1}^2$ and correlation time τ. That is,

$$\dot{b}_1(t) = -\frac{1}{\tau}b_1(t) + w_{b_1}. \tag{9}$$

The variable w_{b_1} is the driving process noise. The statistics of the process modeled by (9) are completely described by the standard deviation σ_{b_1} and the time constant τ. This is because the power spectral density of the driving process noise $Q_{w_{b_1}}$ is related to the variance $\sigma_{b_1}^2 = \mathcal{E}\{b_1^2\}$ and time constant by the following relation [16]:

$$Q_{w_{b_1}} = \frac{2\sigma_{b_1}^2}{\tau}. \tag{10}$$

The sampling noise term $b_w(t)$ is sometimes called "output noise" on sensor specification sheets and can be accurately modeled as band-limited white noise. The band limit for $b_w(t)$ is very high relative to the frequency content of $b_1(t)$. The contribution of $b_w(t)$ to the output error is quantified by σ_{b_w} which is the standard deviation of the sampled measurement noise. In other words, it is the standard deviation of the sensor output when subjected to a zero input and sampled at a rate much higher than the maximum frequency content of $b_1(t)$.

Methods used for determining the numerical values of σ_1, τ, and σ_{b_w} are not discussed in this paper. The interested reader can find a detailed treatment of this subject in [15] and a summary of those results in Table I. This table presents error models for some typical low-performance rate gyros. The first two entries in the table are rate gyros with a quartz vibrating structure sensing elements. The last entry in the table is a fiber-optic gyro (FOG).

TABLE I
Summary of Error Model Parameters for Low-Performance Rate Gyros

Rate Gyro	$b_w(t)$ = Wideband Noise	$b_1(t)$ = 1st Order Gauss-Markov
Systron-Donner "Horizon"	$\sigma_{b_w} = 0.05$ deg/s	$\sigma_{b_1} = 0.05$ deg/s $\tau = 1000$ s
Crossbow DMU-6X	$\sigma_{b_w} = 0.05$ deg/s	$\sigma_{b_1} = 0.05$ deg/s $\tau = 300$ s
FOGs (KVH Autogyro and Crossbow DMU-FOG	$\sigma_w = 0.2$ deg/s	None

The b_0 term from (8) and the s_f term from (7) are not included in Table I because they can be easily estimated (a priori or in real-time) and removed from the gyro output. Furthermore, changes in b_0 and s_f after their initial estimation are comparatively smaller than variations in b_1 [15]. Changes in b_1 and attitude random-walk due to b_w can be large and are the primary contributors to attitude errors.

B. Attitude Error Equations

Since the output errors of the rate gyros are stochastic in nature, one has to perform a covariance analysis to quantitatively assess the performance of an AHRS mechanized using gyros only. If we elect to use Euler angles for this analysis, then the equations required for the covariance analysis are obtained by linearizing (1). Combining the linearization results with the error model given in (9) yields the dynamic system,

$$\delta\dot{\vec{x}} = F\delta\vec{x} + \Gamma\vec{w} \tag{11}$$

where the error state vector $\delta\vec{x}$ is given by

$$\delta\vec{x} = [\delta\psi \quad \delta\theta \quad \delta\phi \quad \delta b_p \quad \delta b_q \quad \delta b_r]^T. \tag{12}$$

The first three entries of $\delta\vec{x}$ represent Euler angle errors while δb_p, δb_q, and δb_r represent errors in our knowledge of the rate gyro biases. The error dynamic matrix F is given by

$$F = \begin{bmatrix} 0 & -\frac{s_\theta}{c_\theta^2}(qs_\phi + rc_\phi) & \frac{qc_\phi - rs_\phi}{c_\theta} & 0 & \frac{s_\phi}{c_\theta} & \frac{c_\phi}{c_\theta} \\ 0 & 0 & -(qs_\phi + rc_\phi) & 0 & c_\phi & -s_\phi \\ 0 & \frac{(qs_\phi + rc_\phi)}{c_\theta^2} & \frac{s_\theta}{c_\theta}(qc_\phi - rs_\phi) & 1 & \frac{s_\phi s_\theta}{c_\theta} & \frac{c_\phi s_\theta}{c_\theta} \\ 0 & 0 & 0 & -\frac{1}{\tau} & 0 & 0 \\ 0 & 0 & 0 & 0 & -\frac{1}{\tau} & 0 \\ 0 & 0 & 0 & 0 & 0 & -\frac{1}{\tau} \end{bmatrix} \tag{13}$$

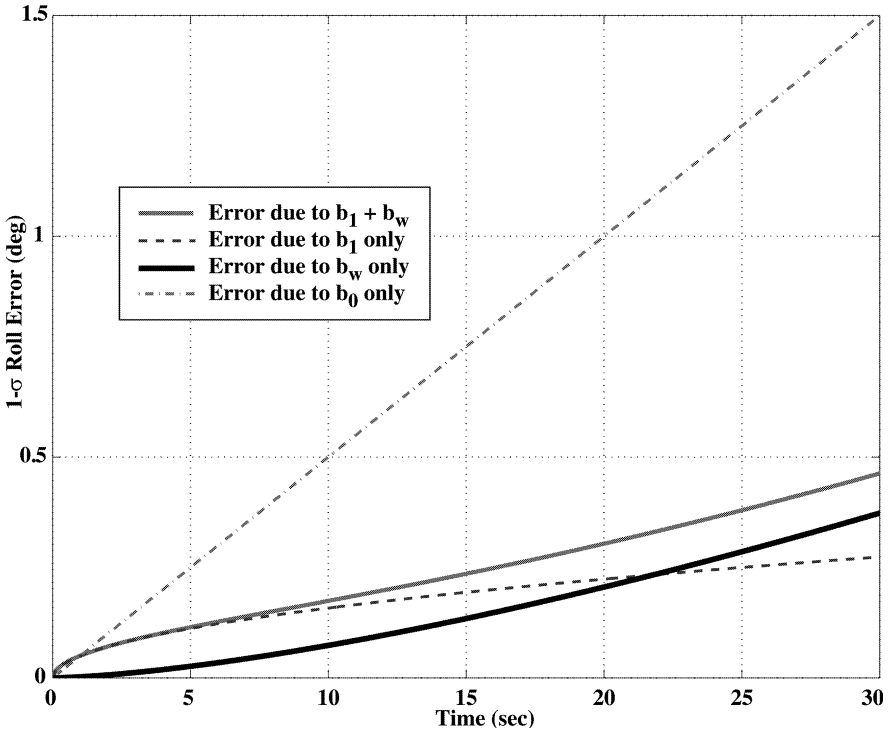

Fig. 2. Effect of gyro output errors on roll Euler angle error.

where τ is the time constant for the gyro bias error. The process noise mapping matrix Γ is given by

$$\Gamma = \begin{bmatrix} F(1:3,4:6) & 0_{3\times3} \\ 0_{3\times3} & I_{3\times3} \end{bmatrix} \tag{14}$$

and relates the process noise vector $\vec{w}$, to $\delta\vec{x}$. The process noise vector $\vec{w}$ is given by

$$\vec{w} = [n_p \quad n_q \quad n_r \quad w_p \quad w_q \quad w_r]^T. \tag{15}$$

The first three entries of $\vec{w}$ represent the wideband measurement errors on the p, q, and r gyro outputs. The last three entries of $\vec{w}$ are the driving noise terms for the stochastic gyro biases (i.e., the equivalent of w_{b_1} in (9)). Thus, the power spectral density matrix for $\vec{w}$ is denoted Q_w and is given by

$$Q_w = \begin{bmatrix} \sigma_p^2 & 0 & 0 & 0 & 0 & 0 \\ 0 & \sigma_q^2 & 0 & 0 & 0 & 0 \\ 0 & 0 & \sigma_r^2 & 0 & 0 & 0 \\ 0 & 0 & 0 & \dfrac{2\sigma^2_{w_p}}{\tau_{w_p}} & 0 & 0 \\ 0 & 0 & 0 & 0 & \dfrac{2\sigma^2_{w_q}}{\tau_{w_q}} & 0 \\ 0 & 0 & 0 & 0 & 0 & \dfrac{2\sigma^2_{w_r}}{\tau_{w_r}} \end{bmatrix}. \tag{16}$$

Numerical values for σ_p, σ_q and σ_r depend on the type of gyro being used and can be found under the second column of Table I. Similarly, numerical values for σ_{w_p}, σ_{w_q}, and σ_{w_r} are found under the second column of Table I. The state error covariance matrix at time step k, P_k, is defined to be $\mathcal{E}\{\delta\vec{x}_k\delta\vec{x}_k^T\}$ and is propagated forward in time by the following relation:

$$P_{k+1} = \Phi_k P_k \Phi_k^T + C_d. \tag{17}$$

The variable Φ_k is the discrete equivalent of the matrix F at time step k and C_d is the discrete equivalent of $\Gamma Q_w \Gamma^T$. Computation of C_d is accomplished using standard methods discussed in [17].

C. Covariance Analysis Results

In the analysis that follows we are interested in the best performance that can be expected from an AHRS that uses low-performance rate gyros only. Thus, we assume that an vehicle equipped with such an AHRS mechanized using a DMU-6X rate gyro triad. The vehicle is assumed to be traveling straight and level ($\theta = \phi = 0°$) on a northerly heading ($\psi = 0°$). For initial conditions we assume that all states except for the roll gyro constant null-shift are known perfectly. The inital variance for the roll gyro null-shift P_{44} is set to $(0.05 \text{ deg/s})^2$. Even though a roll gyro bias will lead to errors in all three Euler angles (due to the coupling of the differential equations), here we only look at the roll error.

The results from the covariance analysis are shown in Fig. 2. As can be seen, when mechanizing an AHRS using low-performance rate gyros alone, the resulting attitude errors are unbounded and grow

rapidly. The largest error is due to the constant null-shift b_0. The effect of the null-shift can be mitigated, however, because it is rather easy to estimate its magnitude a priori or in real-time using estimators that are described later in this paper. In the absence of a large null-shift, what becomes problematic are the stochastic errors $b_1(t)$ and $b_w(t)$. In the absence of the uncompensated null-shift b_0, Fig. 2 shows that the the attitude error growth is dominated by the contributions of the $b_1(t)$ term. Although the attitude errors due to integration of wide band noise are smaller than the errors due to the bias instability, they are not negligible.

As solid-state sensor technology improves, it is conceivable that the correlated error term $b_1(t)$ will become very small, and thus, its contribution to attitude errors less significant. However, as long as there is wideband noise on the sensor output (either inherent to the sensor itself or due to external causes such as vehicle vibration, power supply noise, etc.,) attitude drift will be present.

III. AIDING SYSTEMS

Even though open-loop integration of low-performance rate gyros leads to unbounded attitude errors as shown in Fig. 2, these sensors have good high-bandwidth response. This feature makes them attractive for many AHRS applications where high bandwidth attitude information is indispensable. Attitude drift errors resulting from gyro output errors can be eliminated if an attitude sensor (or system) with bounded errors is used to aid the gyros. The aiding system can be used to periodically "reset" the attitude solution derived from the inexpensive rate gyros. Sensor fusion techniques such as Kalman filtering can be used to blend the rate gyros and aiding system outputs. In this paper two aiding systems are considered. The first one is a multi-antenna, carrier-phase differential GPS (CDGPS) attitude determination system. The second aiding system consists of a magnetometer triad and two accelerometers.

In most AHRS applications, these aiding systems cannot be used alone because they have limited bandwidth (which is the case for multi-antenna GPS systems) or cannot be relied on to give an accurate attitude solution during certain aircraft maneuvers (which is the case for both GPS as well as accelerometer and magnetometer based systems). To see why this is the case, first let us consider the multi-antenna GPS attitude determination systems. The basic idea behind GPS attitude determination is the mathematical fact that three noncollinear points in space define a plane. If the location of these three points with respect to some predefined reference frame is known, then the orientation of the plane containing the three points can be computed. In practical terms, if three noncollinear GPS antennas are mounted on a rigid plane (e.g., the fuselage of an airplane) and the relative location of the antennas with respect to each other on the rigid plane is known, then the attitude of the rigid plane containing these antennas can be determined. The relative location of the three antennas can be measured accurately using CDGPS techniques [9, 18, 10]. One of the limitations of GPS attitude determination systems is that that the rate at which the attitude solution is generated is a function of how often a GPS measurement is available. Normally, the maximum data output rate from currently available GPS receivers is on the order of 10 Hz. Most AHRS applications require update rates much higher than 10 Hz.

In a magnetometer and accelerometer aiding system, the measurements required to compute pitch and roll come from a pair of accelerometers. Heading or yaw is computed using measurements obtained from a magnetometer triad and the pair of accelerometers. The accelerometers are arranged with their sensitive axes perpendicular to each other. Furthermore, they are mounted in an airplane such that one of the accelerometer has its sensing axis aligned with the longitudinal axis of the airplane. The other accelerometer's sensing axis is aligned with the airplane's lateral axis. If we use f_x to represent measurements from the accelerometer aligned with the longitudinal axis of the airplane (in units of g) and f_y for measurements from the accelerometer aligned with the lateral axis of the airplane, then pitch and roll are computed using the following expressions:

$$\theta = -\sin^{-1}(f_x) \tag{18}$$

$$\phi = \sin^{-1}(f_y). \tag{19}$$

The computed pitch and roll can be used to form a transformation matrix which map the magnetometer measurements from a coordinate frame in the body of the airplane to the locally level tangent plane. After this transformation, heading or yaw is computed using the following relation:

$$\psi = -\tan^{-1}\left(\frac{B_y^b}{B_x^b}\right) \tag{20}$$

where B_y^b and B_x^b are components of Earth's magnetic field vector measured by the longitudinal and lateral axis magnetometers, respectively.

During maneuvers where the aircraft is accelerating, there will be an error in the accelerometer derived attitude for pitch and roll. This is because the sensing element of an accelerometer is a pendulous mass and, therefore, cannot distinguish the difference between tilt and acceleration. Therefore, in an AHRS that uses a magnetometer-accelerometer

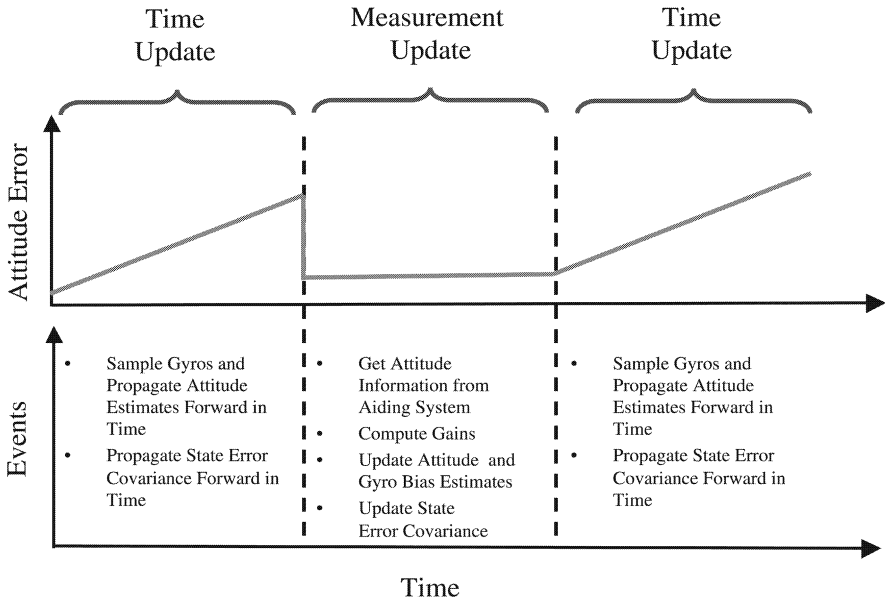

Fig. 3. Time line for attitude estimator.

aiding system, only the attitude solution generated by the rate gyros can be relied on during maneuvers involving accelerations or decelerations.

IV. SENSOR FUSION OVERVIEW

An AHRS that uses sensor fusion techniques to blend rate gyro and aiding system outputs was shown schematically in Fig. 1. The system depicted in Fig. 1 is an estimator and Fig. 3 is a time line showing (qualitatively) how the estimation algorithms work. After the initial conditions for the attitude are established, the rate gyros are integrated to propagate the attitude estimate forward in time. The process of propagating attitude forward in time is called the "time update" and is carried out at a relatively high rate. The time update provides the high-bandwidth attitude information. Such information is needed, for example, in applications such as pilot-in-the-loop control of manned aircraft. Because of gyro output errors, however, the computed attitude solution will drift with time. This is shown in the top graph of Fig. 3 and implies that the attitude solution obtained by integrating the rate gyros cannot be propagated indefinitely without periodic resets. A periodic reset, called the "measurement update," occurs when an attitude estimate from the aiding system becomes available. The gyro biases are also estimated at the measurement update. After a measurement update, a new time update phase begins and cycle repeats.

V. SENSOR FUSION ALGORITHMS

We now present the mathematical details for mechanizing the estimators discussed earlier. First we discuss an Euler angle based estimator. This is followed by a similar discussion for a quaternion-based estimator.

For the Euler angle estimator, the state vector of interest $\vec{x}$ is given by

$$\vec{x} = [\psi \quad \theta \quad \phi \quad b_p \quad b_q \quad b_r]^T. \tag{21}$$

The system of differential equations relating Euler angles to rate gyro outputs is nonlinear and mechanizing an attitude estimator requires linearizing this system of equations. Linearzing yields a system of equations that it is in the form of (11). The state vector for this linearized system $\delta\vec{x}$ is a perturbation of $\vec{x}$ and is given by (12). Thus, the dynamic model for this estimator is identical to the one used earlier in the open-loop covariance analysis except for one detail. The process noise mapping matrix Γ in this case is given by

$$\Gamma = \begin{bmatrix} \alpha F(1:3,4:6) & 0_{3\times 3} \\ 0_{3\times 3} & \beta I_{3\times 3} \end{bmatrix}. \tag{22}$$

The variables α and β are tuning parameters that are discussed later. Even though this dynamic model includes a mathematical expression for the time rate of change for the rate gyro biases, the model is a stochastic one and cannot be used to deterministically propagate the gyro biases forward in time. It is only used for propagating the gyro bias estimate covariance. The rate gyro biases are estimated during the measurement update. Similarly, only the the Euler angle error covariance is propagated using (11)–(15). Unlike the gyro biases, however, the Euler angles themselves are propagated forward time (and in parallel with the state error covariance) by numerically integrating the nonlinear Euler angle

kinematic relation given by (1). At each measurement update, the Euler angles are adjusted to account for attitude errors that accumulate during the process of integrating (1) between measurement updates. These errors are primarily due to rate gyro biases and wideband noise.

As was noted in the discussion associated with Fig. 3 the measurement update occurs at a slower rate than the time update. The measurement update equation that is used once at each measurement update is given by

$$\delta\vec{x}_k^{(+)} = L_k(\vec{y}_k - H\hat{\vec{x}}_k^{(-)}) = L_k(\vec{y}_k - \hat{\vec{y}}_k) = L_k\delta\vec{y}_k. \quad (23)$$

The "−" superscript indicates a quantity before the measurement update and "+" superscript indicates a quantity after the measurement update. The measurement vector $\vec{y}_k$ is given by

$$\vec{y}_k = [\psi_{\text{AS}} \quad \theta_{\text{AS}} \quad \phi_{\text{AS}}]_k^T. \quad (24)$$

The subscript AS stands for aiding system because $\vec{y}_k$ is composed of the Euler angle estimates from the aiding system. The elements of the predicted measurement vector $\hat{\vec{y}}_k$ are estimates of the three Euler angles at time step k. These estimates are nothing more than the Euler angles computed by integrating (1) forward in time since the last measurement update. At each measurement update, the estimator gain (Kalman gain) matrix L_k and the updated state covariance matrix $P_k^{(+)}$ are computed using the following relations [17, 19]:

$$L_k = P_k^{(-)}H^T(H^TP_k^{(-)}H + R_v)^{-1} \quad (25)$$

$$P_k^{(+)} = (I_{6\times6} - L_kH)P_k^{(-)}. \quad (26)$$

In a real-time implementation of these algorithms, the Kalman gain matrix does not have to be computed at each measurement update. Instead, the steady state value of the gain, computed a priori, is used in accordance with a gain schedule. This issue of gain scheduling is discussed later.

The measurement matrix H is defined as

$$H = [I_{3\times3} \quad 0_{3\times3}]. \quad (27)$$

The variable R_v is the measurement noise covariance matrix and is defined as follows:

$$R_v = \begin{bmatrix} \sigma_\psi^2 & 0 & 0 \\ 0 & \sigma_\theta^2 & 0 \\ 0 & 0 & \sigma_\phi^2 \end{bmatrix}. \quad (28)$$

The diagonal entries in (28) are the wideband noise on the measurements of ψ, θ, and ϕ from the aiding system. Numerical values for these entries are obtained from the aiding system error models.

After each measurement update, the Euler angle and bias states are updated as follows:

$$\psi_k^{(+)} = \psi_k^{(-)} + \delta x_k^{(+)}(1) \quad (29)$$

$$\theta_k^{(+)} = \theta_k^{(-)} + \delta x_k^{(+)}(2) \quad (30)$$

$$\phi_k^{(+)} = \phi_k^{(-)} + \delta x_k^{(+)}(3) \quad (31)$$

$$b_{p,k}^{(+)} = b_{p,k}^{(-)} + \delta x_k^{(+)}(4) \quad (32)$$

$$b_{q,k}^{(+)} = b_{q,k}^{(-)} + \delta x_k^{(+)}(5) \quad (33)$$

$$b_{r,k}^{(+)} = b_{r,k}^{(-)} + \delta x_k^{(+)}(6) \quad (34)$$

where $\delta x_k^{(+)}(i)$ is the ith component of $\delta\vec{x}_k^{(+)}$.

For the system where the attitude parameterization is in the form of quaternions, the state vector is given as follows:

$$\delta\vec{x} = [\vec{q}_e \quad \delta b_p \quad \delta b_q \quad \delta b_r]^T. \quad (35)$$

The first entry is a quaternion error vector while the remaining three entries represent the error in our knowledge of the roll, pitch and yaw axis gyro biases, respectively. To understand the meaning of $\vec{q}_e$ in (35), consider $\hat{\mathbf{q}}$, which is an estimate of the true attitude quaternion $\mathbf{q}$. The small rotation from the estimated attitude $\hat{\mathbf{q}}$, to the true attitude is defined as $\mathbf{q}_e$. This is the error quaternion which is small but non-zero. It is non-zero because of the rate gyro output errors and the relationship between $\mathbf{q}_e$, $\hat{\mathbf{q}}$, and $\mathbf{q}$ is given by

$$\mathbf{q} = \hat{\mathbf{q}} \otimes \mathbf{q}_e. \quad (36)$$

The symbol $\otimes$ indicates quaternion multiplication [14]. The error quaternion $\mathbf{q}_e$ is assumed to represent a small rotation. Thus, in view of the quaternion definition given in (4), $\mathbf{q}_e$ can be approximated as

$$\mathbf{q}_e = [1 \quad \vec{q}_e^T]^T. \quad (37)$$

The time update equation used with the quaternion mechanization of an AHRS is written in the standard state-space form given by (11) where the system dynamics matrix F is defined as

$$F = \begin{bmatrix} -[\vec{\omega}^\times] & \frac{1}{2}I_{3\times3} \\ I_{3\times3} & -\frac{1}{\tau}I_{3\times3} \end{bmatrix}. \quad (38)$$

The vector $\vec{\omega}$ is equal to $[p \;\; q \;\; r]^T$ and $[\vec{\omega}^\times]$ is the skew symmetric matrix composed from the entries in $\vec{\omega}$. The process noise mapping matrix Γ is given by

$$\Gamma = \begin{bmatrix} -\alpha\frac{1}{2}I_{3\times3} & 0_{3\times3} \\ 0_{3\times3} & \beta I_{3\times3} \end{bmatrix}. \quad (39)$$

The interested reader can refer to [11] for a discussion of how this dynamic model is derived. The process noise vector $\vec{w}$ is identical to the one used in the Euler angle mechanization and is given by (15). Thus, the process noise power spectral density matrix Q_w for the quaternion implementation is identical to the one used

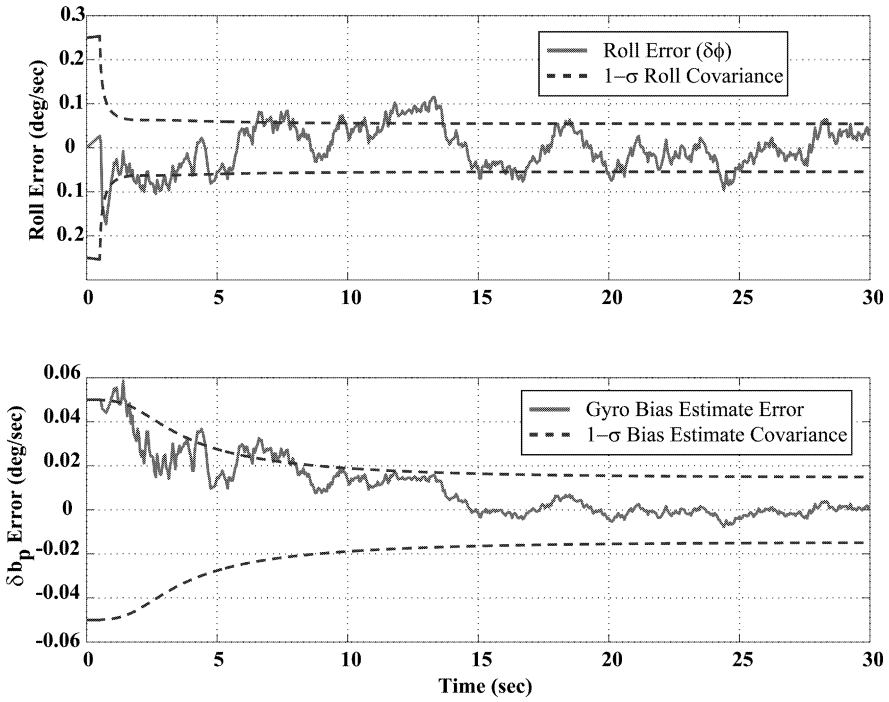

Fig. 4. Roll angle and gyro bias estimation error and standard deviation.

with the Euler angle implementation given by (16). Similar to the Euler angle mechanization, this dynamic model is used only for propagating the covariance of $\delta\vec{x}$. The estimated attitude quaternion $\hat{\mathbf{q}}$ is propagated separately using (2) and updated at each measurement update using information from the aiding system.

The measurement update equation is given by

$$\delta\hat{\vec{x}}_k^{(+)} = L_k(\vec{y} - \hat{\vec{y}}_k) = L_k\delta\vec{y}_k. \tag{40}$$

The vector $\vec{y}_k$ is equal to the vector part of the difference (in the quaternion sense) between the aiding system's computed and filter's estimated attitudes. In other words, it is nothing more than the vector component of $\hat{\mathbf{q}}_e^{(-)}$ before the measurement update and is computed using the following relation:

$$\hat{\mathbf{q}}_e^{(-)} = [1 \quad (\hat{\vec{q}}_e^{(-)})^T]^T = \mathbf{q}_{\text{AS}} \otimes \hat{\mathbf{q}}^{(-)} \tag{41}$$

where $\mathbf{q}_{\text{AS}}$ is the attitude quaternion as computed by the aiding system. Thus,

$$\delta\vec{y}_k = \hat{\vec{q}}_e^{(-)}. \tag{42}$$

After $\delta\hat{\vec{x}}_k^{(+)}$ is computed, the attitude quaternion and rate gyro biases are updated as follows:

$$\hat{\mathbf{q}}^{(+)} = \hat{\mathbf{q}}^{(-)} \otimes [1 \quad \delta\hat{x}_k^{(+)}(1) \quad \delta\hat{x}_k^{(+)}(2) \quad \delta\hat{x}_k^{(+)}(3)]^T \tag{43}$$

$$b_{p,k}^{(+)} = b_{p,k}^{(-)} - \delta x_k^{(+)}(4) \tag{44}$$

$$b_{q,k}^{(+)} = b_{q,k}^{(-)} - \delta x_k^{(+)}(5) \tag{45}$$

$$b_{r,k}^{(+)} = b_{r,k}^{(-)} - \delta x_k^{(+)}(6). \tag{46}$$

To ensure that $\hat{\mathbf{q}}^{(+)}$ has a magnitude of unity, after each measurement update it is normalized in the following manner:

$$(\hat{\mathbf{q}}^{(+)})_{\text{normalized}} = \frac{\hat{\mathbf{q}}^{(+)}}{\|\hat{\mathbf{q}}^{(+)}\|}. \tag{47}$$

VI. CLOSED-LOOP PERFORMANCE

To quantify the improvement in performance gained when rate gyros are fused with an aiding system, we repeat the covariance analysis presented earlier in Fig. 2. We consider an Euler angle mechanization because the results are more intuitive and easier to interpret. Furthermore, from the standpoint of performing a covariance analysis, there is no difference between an Euler angle and quaternion implementation. In this simulation we include an aiding system in the form of a multi-antenna GPS attitude determination system which generates a bias free attitude solution corrupted by wideband noise only . The standard deviation of the wideband noise is the same for yaw, pitch, and roll ($\sigma_\psi = \sigma_\theta = \sigma_\phi$) and has a magnitude of 0.25° [10]. The rate gyros are sampled at 20 Hz and the attitude solution is propagated forward in time at the same rate. The GPS attitude determination system generates estimates of the three Euler angles at a 2 Hz rate. The tuning parameters α and β are set to 1.

Fig. 4 shows the performance obtained with this attitude estimator. The figure shows the 1σ standard deviation bounds for the roll error. Consistent with our earlier claims, the figure shows that the aided system

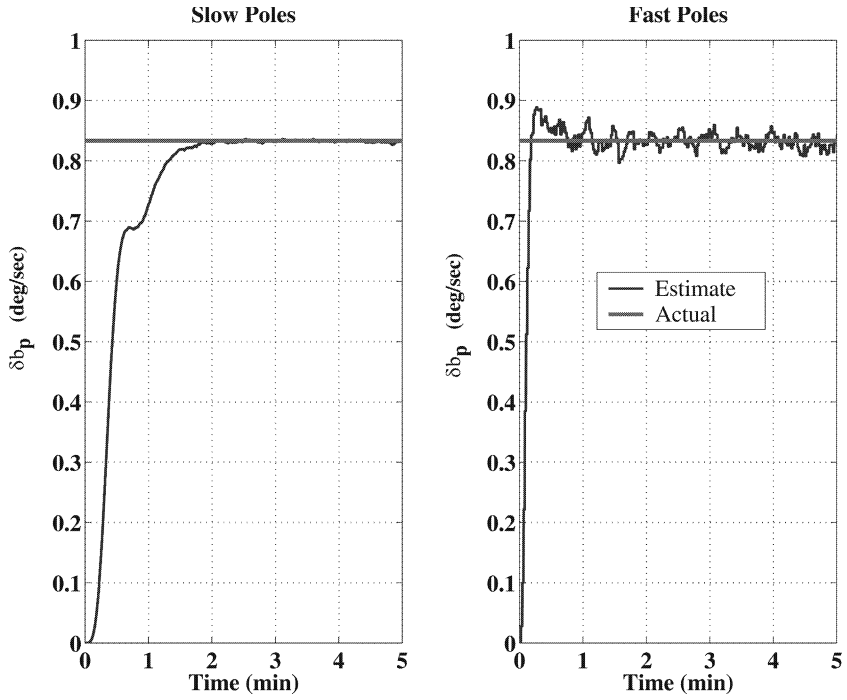

Fig. 5. Effect of pole speed on rate gyro bias estimation.

has bounded errors. The steady state 1σ attitude error is smaller than the 0.25° noise of the aiding system error. Thus, the blended solution performs better than either the gyro derived solution or that of the aiding system alone. Also shown is the 1σ standard deviation bound for the error in the roll gyro bias estimate. Again, the uncertainty of the bias estimate is seen to be reduced below the values of σ_{b_1} and σ_{b_w} for this particular gyro. Fig. 4 also shows a trace of the actual attitude error and bias estimates for one particular run of this simulation. As can be seen, even though the attitude and bias errors are bounded, the actual attitude and bias estimates are noisy.

VII. ESTIMATOR TUNING

A noisy or jittery attitude solution is acceptable in some applications but undesirable when an AHRS is used for pilot-in-the-loop control. In these instances, the attitude noise can be reduced by setting the tuning parameters α and β to values other than unity. There is an important trade-off involved in selecting values for these tuning parameters because the location of the estimator poles are controlled by them. Larger values of α and β result in faster poles. Fast estimator poles result in large gains and slow estimator poles result in small gains. Thus, larger values of α and β lead to faster convergence of the state estimates. Furthermore, an examination of (22) and (39) shows that α controls the poles associated with the Euler angle or quaternion error states, respectively, while β controls the poles associated with the gyro biases.

Simply, increasing the values of α and β to get a faster convergence results in a noisier attitude solution like that shown in Fig. 4. It is possible to increase the value of β only which would speed up the convergence of the gyro bias estimates without significantly magnifying the noise on the Euler angle (or quaternion) estimates. The problem with this approach is that it results in a noisy (or poor) gyro bias estimates which affect the ability of the estimator to coast through a temporary unavailability of the aiding system (e.g., brief GPS outages).

Fig. 5 shows the results of a simulation study evaluating the trade-off involved in choosing the speed of the estimator poles. The values for various estimator parameters are shown in Table II. The heavy solid trace in Fig. 5 is the actual value of the roll gyro bias. The thin solid trace in the left plot of Fig. 5 shows the roll gyro bias estimate generated by an estimator using slow poles. The thin solid trace in the right plot shows an estimate of the same state using an estimator with faster poles. As would be expected, the use of faster poles speeds up the convergence of the bias state estimate but leads to a much noisier solution.

VIII. GAIN SCHEDULING

For attitude determination systems mechanized using low-performance gyros, the accuracy of the attitude solution is ultimately a function of the aiding system's accuracy. This is because as shown in Fig. 2 the attitude error when using rate gyros alone is unbounded. Thus, there is little difference in accuracy whether the implementation is done using Euler angles or quaternions. From an estimator and practical

TABLE II
Estimator Pole Trade-Off Study. Numerical Values for Euler Angle Filter

Matrix	Matrix Parameter	Numerical Values		Relevant Equation(s)
		Slow Poles	Fast Poles	
R_v	σ_ψ σ_θ σ_ϕ	0.25°	0.25°	Equation (28)
Q_w (Wideband)	α	10	10	Equation (22)
	σ_p σ_q σ_r	0.05°/s	0.05°/s	Equations (8) and (16)
Q_w (Correlated)	β	1	10	Equation (22)
	σ_w	0.05°/s	0.05°/s	Equations (8), (10) and (16)

system design standpoint, however, the quaternion implementation of the filter has three advantages over a Euler angle formulation. Firstly, the well-known problem of "gimbal lock" (Euler angle singularity at $\theta = \pm 90°$) is eliminated when using quaternions. This is not necessarily a significant advantage, however, because extreme maneuvers where an aircraft's pitch angle exceeds $\pm 90°$ are rare. The second advantage is that the time update equations for the quaternion implementation do not involve transcendental functions. As such, computations with the quaternion filter can be executed at a faster rate using inexpensive microprocessors with limited computational power. The third advantage is also related to computational speed and it is that estimator gain scheduling is easier when using quaternions.

To see why gain scheduling is easier when using quaternions, we write out the measurement update equation as follows:

$$\hat{\vec{x}}^{(+)} - \hat{\vec{x}}^{(-)} = \delta\vec{x} = L(\vec{y} - H\hat{\vec{x}}) = L\delta\vec{y}. \tag{48}$$

From (48) it can be seen that the gain matrix is the "constant of proportionality" (or more appropriately a matrix of Jacobians) that maps the innovations process $\delta\vec{y}$ into the state error vector $\delta\vec{x}$. In the Euler angle mechanization, the three elements of the innovations process are the differences between the aiding system's attitude solution and the filter's estimate of attitude before a measurement update. That is,

$$\delta\vec{y} = \begin{bmatrix} \psi_{\text{AS}} - \hat{\psi}^{(-)} \\ \theta_{\text{AS}} - \hat{\theta}^{(-)} \\ \phi_{\text{AS}} - \hat{\phi}^{(-)} \end{bmatrix} = \begin{bmatrix} \Delta\psi \\ \Delta\theta \\ \Delta\phi \end{bmatrix}. \tag{49}$$

The innovation process $\delta\vec{y}$ for the quaternion mechanization is given by

$$\delta\vec{y} = \hat{\vec{q}}_e^{(-)} = \begin{bmatrix} q_e^{(-)}(1) \\ q_e^{(-)}(2) \\ q_e^{(-)}(3) \end{bmatrix}. \tag{50}$$

Now it is clear to see that in the Euler angle mechanization the mapping of the innovations process into the first three entries of the state error vector should be one to one. That is, yaw innovations should map into yaw state errors, and the same for pitch and roll. More importantly, this mapping is independent of attitude. This situation is different for the mapping of the innovations process into the gyro bias estimate errors. This can be seen mathematically by examining (13). The submatrix formed by the first three rows and last three columns of F maps gyro biases into Euler angles. This matrix is a function of the current Euler angle estimates. Thus, the mapping of the innovation process into gyro bias estimate must also be a function of the current attitude estimate. For example, if the AHRS is level, then the yaw innovations map into yaw gyro biases, pitch innovations map into pitch gyro biases and roll innovations map into roll gyro biases. At an attitude other than level, this mapping will change. For the quaternion mechanization, provided the pitch angles and angular rates are small, all the mappings of the innovations process to gyro bias estimate errors are constant and independent of the estimated attitude. This is because in the quaternion mechanization, the innovations process represents errors in the estimate of the quaternion error vector $\vec{q}_e$. The quaternion error $\vec{q}_e$ is small and its elements are nothing more than the rotation errors about the roll, pitch, and yaw axes of the aircraft, respectively. This can be seen by examining the dynamic matrix F given by (38).

Figs. 6, 7, and 8 show the results of a simulation study performed to assess the dependence of the gyro bias gains on attitude. Fig. 6 shows the time history of the three Euler angles for this simulation. Yaw and pitch are zero for the entire history while roll varies sinusoidally between $+90°$ and $-90°$. For the Euler angle and quaternion mechanizations, the mappings of the innovations process into the roll gyro bias estimate δb_p are shown in the upper-most plots of Figs. 7 and 8, respectively. For both mechanizations, the only non-zero, steady state element of the Kalman gains associated with δb_p is the entry in the fourth row and third column of the matrix L (i.e., L_{43}). For the Euler angle mechanization, this gain maps roll innovations into roll gyro bias estimate errors. The middle plots in Figs. 7 and 8 show the mapping of the innovations process into pitch gyro bias estimate errors δb_q. In Fig. 7 it can be seen that the gains mapping yaw and pitch innovations into δb_q are non-zero and time varying. If we ignore the initial filter transients, we see that the gain mapping yaw innovations into the pitch gyro bias (L_{51}) is zero when $\phi = 0°$ but is maximum when $\phi = 90°$. This indicates that at $\phi = 0°$ the mapping is strictly from pitch innovations to pitch gyro bias estimate errors. At a roll angle of 90°, the mapping changes and becomes from yaw innovations to pitch gyro bias estimate. The bottom-most plots of

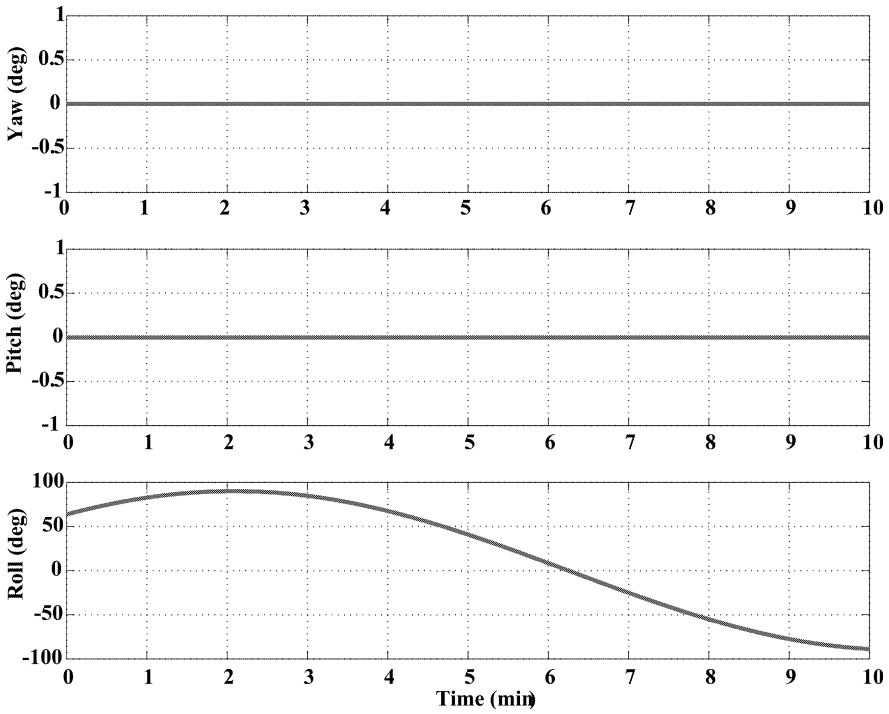

Fig. 6. Euler angle history.

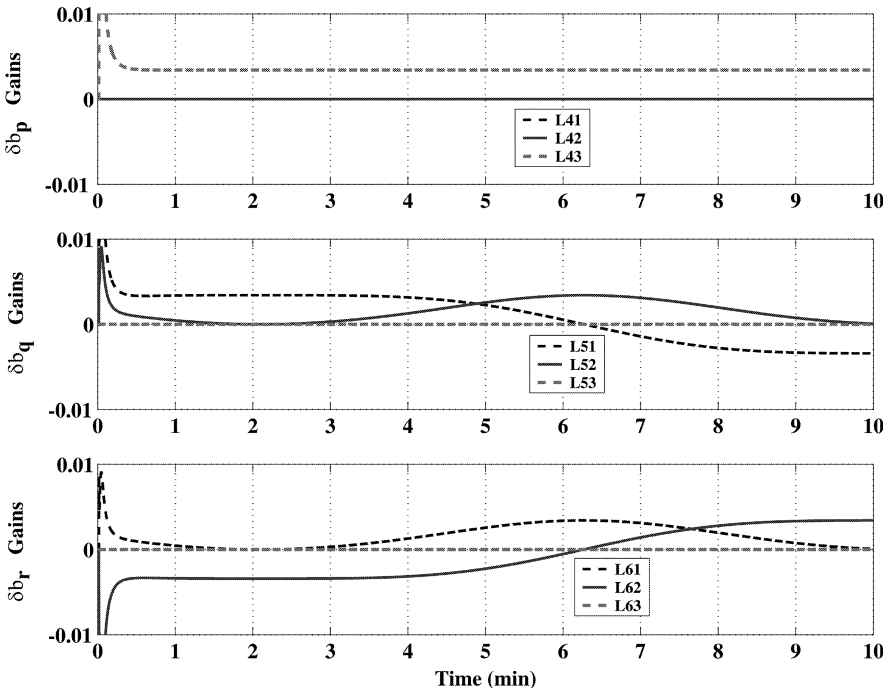

Fig. 7. Gain history for Euler angle filter.

Figs. 7 and 8, show the mapping of the innovations process into the yaw gyro bias estimate errors δb_r. For the Euler angle mechanization the mapping of the innovations process into the yaw gyro bias estimate errors is also a function of roll angle.

From Fig. 8 it is apparent that scheduling gains for a quaternion filter is straightforward because a single steady state gain matrix computed from a given set of α, β, R_v, and Q_w can be used. A more sophisticated gain schedule that uses two gain matrices can also be implemented. The first of these gain matrices would be the steady state gain matrix computed using large values of α and β (or fast poles). It would be used during filter start-up to assure rapid convergence of the attitude solution and rate gyro bias estimates. Once the initial values for the attitude and gyro biases have

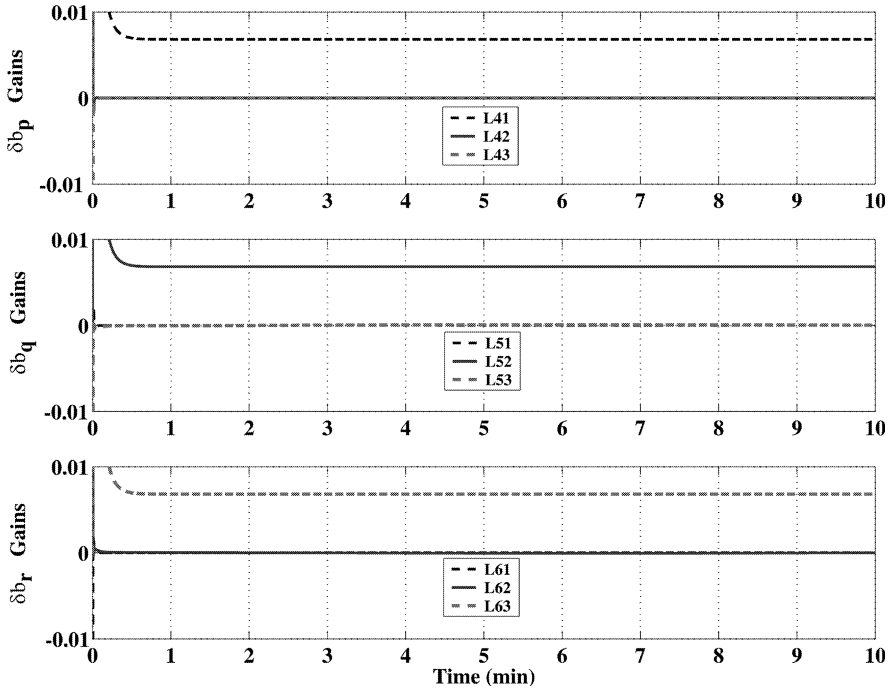

Fig. 8. Gain history for quaternion filter.

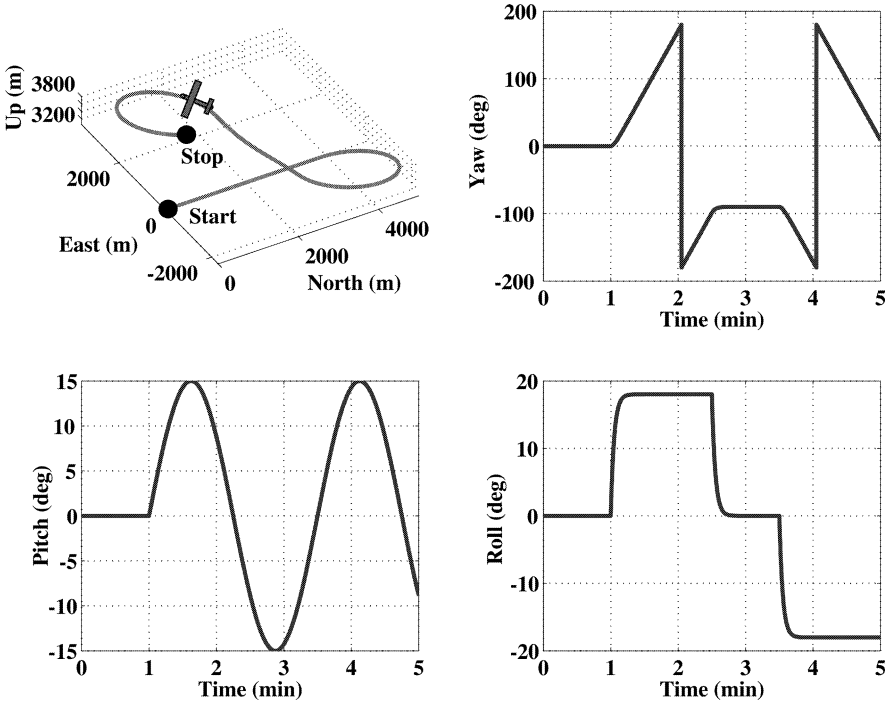

Fig. 9. "Figure-eight" trajectory.

been determined, the filter is switched to a slower set of gains computed using smaller values of α and β.

A similar gain scheduling scheme would not be meaningful for an Euler angle filter because the gain matrix is a function of vehicle attitude. Specifically, unless the dynamic range of pitch and roll are small, the performance of a constant gain Euler angle filter can be poor. The results from the following simulation study show why this is the case. Consider the performance of an attitude estimator in an airplane flying along the two trajectories shown in Figs. 9 and 10. The Euler angle histories associated with these trajectories are also shown in Figs. 9 and 10. The pertinent filter parameters are identical to those given in Table II except that $\alpha = \beta = 1$. The time and measurement updates occur at 20 Hz and 2 Hz, respectively. Note that for the first minute the attitude is constant ($\psi = \theta = \phi = 0°$) for both trajectories.

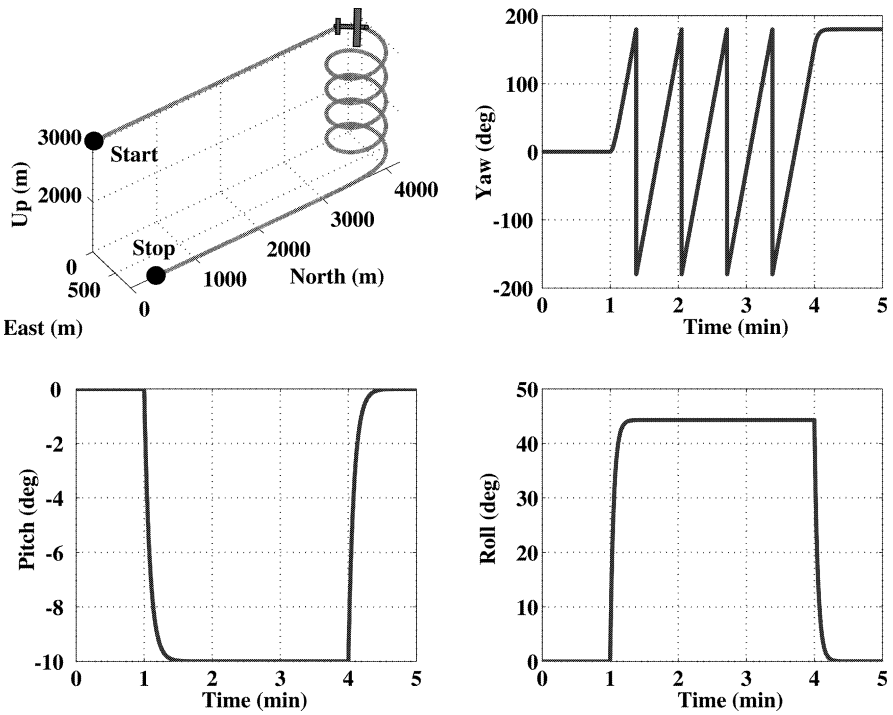

Fig. 10. Spiral trajectory.

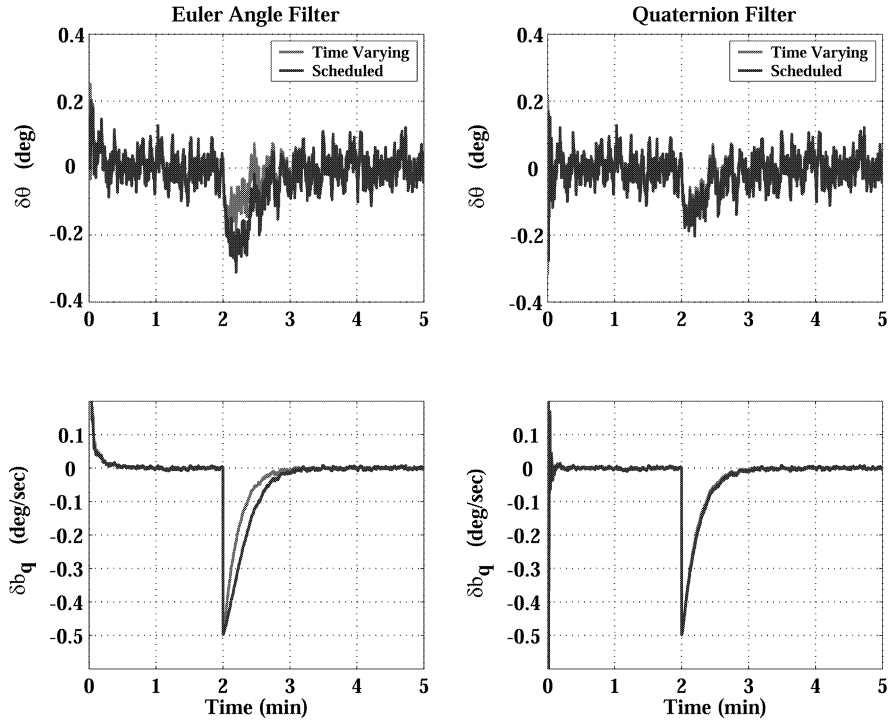

Fig. 11. Pitch and pitch gyro bias estimation errors for "figure-eight" trajectory.

Suppose gains are scheduled such that the steady state gain matrix computed at the end of the first minute is subsequently used for the remainder of either trajectory. We are interested in knowing the effect of this gain schedule on the resulting attitude and gyro bias estimation errors.

As can be seen in Figs. 11 and 12, between $t = 1$ and $t = 2$ min, the the estimation errors in pitch attitude ($\delta\theta$) and pitch gyro bias (δb_q) are small and negligible. This is not surprising because by the end of the first minute when the gains have reached steady state, the attitude errors (that is, the difference between the aiding system and rate gyro derived attitude solutions) are nearly zero and the gyro bias estimates have converged. For the remainder of the flight, the change in the gyro biases is also small. This

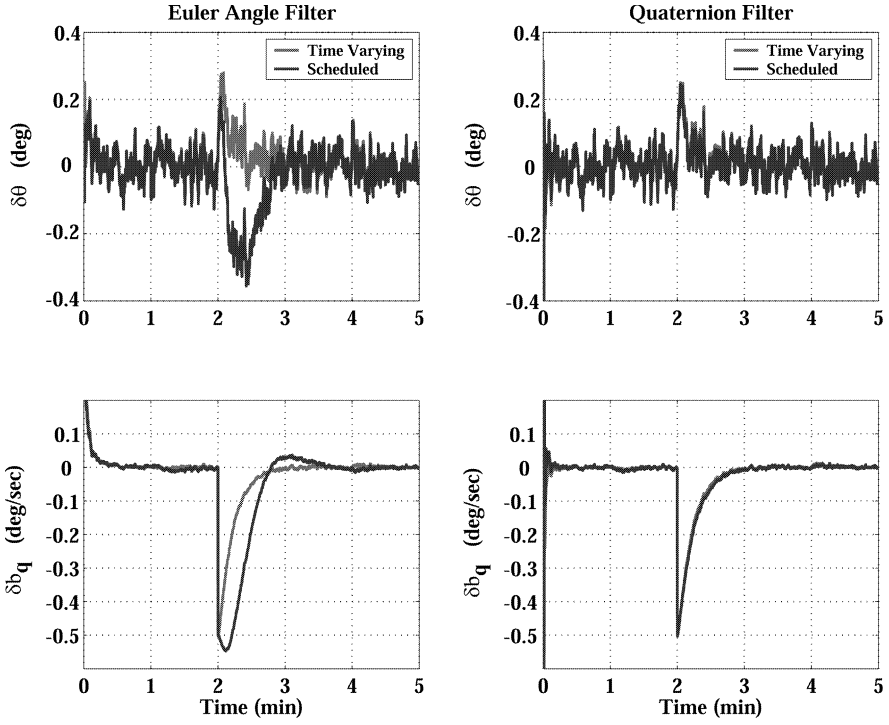

Fig. 12. Pitch and pitch gyro bias estimation errors for spiral trajectory.

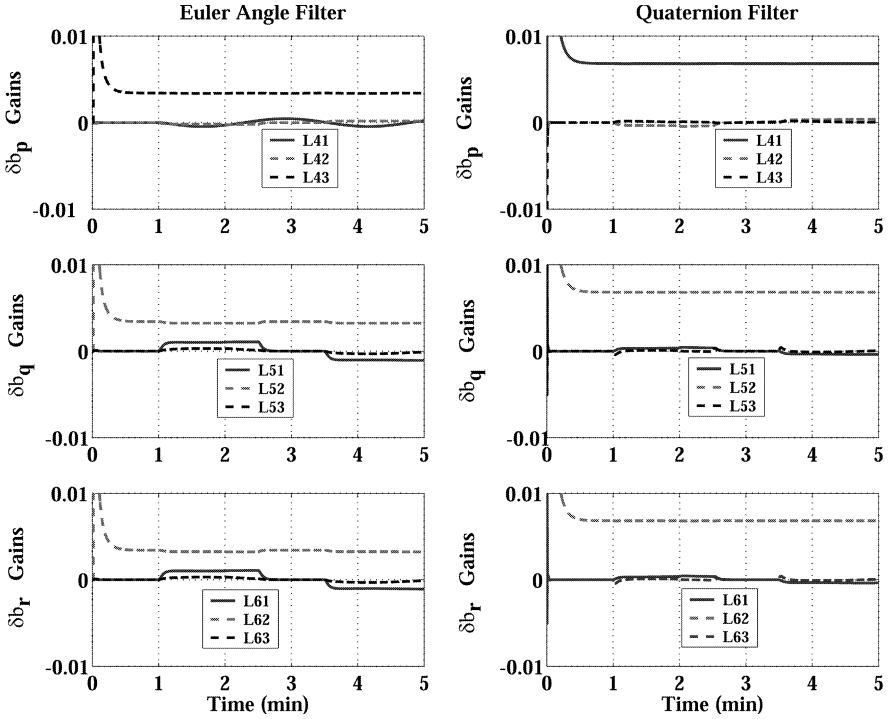

Fig. 13. Gain history for "figure-eight" trajectory.

means that the innovations process will be nearly zero for most of the flight even though the computed gains are changing with attitude as shown in Figs. 13 and 14. As such, although the scheduled constant gains are incorrect when θ and ϕ are non-zero, they are being multiplied by an innovations process vector that is approximately equal to zero. Thus, the resulting attitude and gyro bias solutions are not affected significantly.

The situation is different, however, if there is a rapid (or step) change in gyro bias or attitude after the first minute. Even though such changes are unlikely, it is conceivable that a step change in gyro bias can occur if there is a power interruption and the last

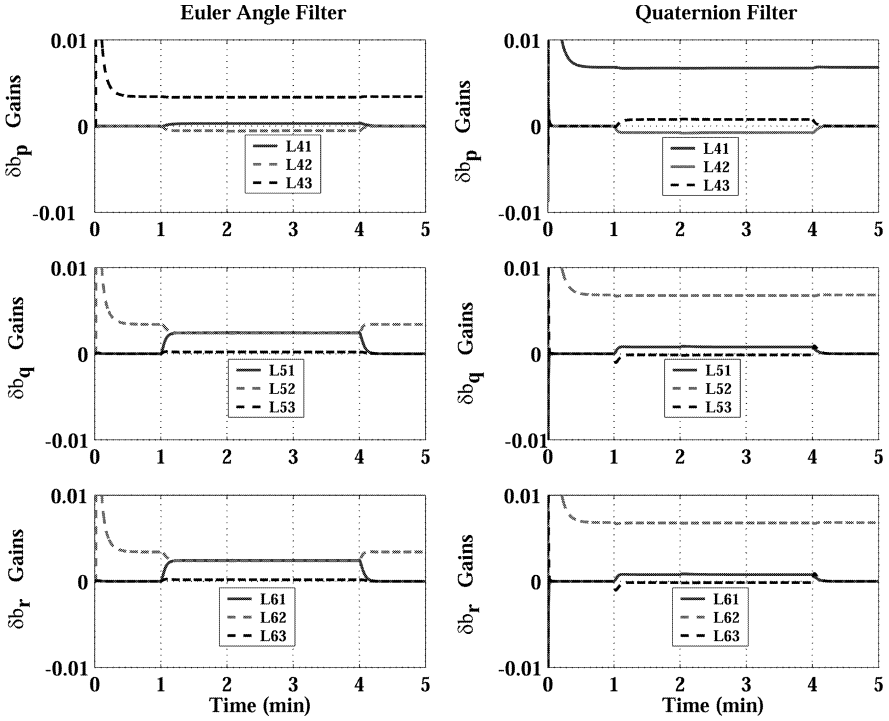

Fig. 14. Gain history for spiral trajectory.

value of estimated bias is not saved. A step change in attitude can result during abrupt maneuvers with frequency content higher than the sensing bandwidth of the rate gyros or integration algorithm. In this case, using constant gains can degrade the performance of the filter. This is what is shown at the $t = 2$ min mark in Figs. 11 and 12. At $t = 2$ min, all three gyros are subjected to a step change in output bias of 0.05 deg/s. Only the pitch attitude and gyro bias estimation errors are shown because the result for the other states is similar. The trace labeled "time varying" corresponds to a filter that uses the gains shown in Figs. 13 and 14 which are computed by solving (17), (25), and (26). Both the time-varying and constant gain filters drive the attitude and gyro bias estimation errors to zero. Even though the constant gain Euler angle filter converged in this case, there is no guarantee that it will do so every time nor that the its performance will be the same. For example, Fig. 12 shows the performance of the same filter during the more severe spiral trajectory. In this case, the estimation errors for the constant gain filter exhibit an overshoot and some ringing.

For the quaternion-based filter, the difference between the constant and time-varying gain mechanizations is almost imperceptible. The slight difference seen is due to the fact that the gains for the quaternion and Euler angle filters are dependent on, albeit weakly, the magnitude of the angular velocity vector. This fact can be seen by observing the dynamic matrix F for both implementations given in (13) and (38). The dynamic matrix F is a function of the angular rates p, q, and r. As such, for completeness, scheduling of the quaternion gains must take into account angular rate as well. This can be seen clearly in Fig. 15 which is similar to Fig. 6 and shows the time history of the three Euler angles. In the case of Fig. 15, however, the magnitude of the maximum angular rate is twice of that shown in Fig. 6. Fig. 16 shows the gain history for the quaternion mechanization associated with the attitude history shown in Fig. 16. The gains that map $q_e(1)$, $q_e(2)$, and $q_e(3)$ into δb_p, δb_q, and δb_r respectively, are still constant and larger compared with the other gains. The other gains are non-zero but much smaller in comparison and, thus, their effect not very significant in many practical applications as can be seen in Figs. 11 and 12.

In summary, while constant gains can be used with Euler angle and quaternion-based filters, quaternions will give a better performance because the gains are unaffected by attitude and only weakly affected by angular rate.

IX. EXPERIMENTAL VALIDATION

Experimental validation of these attitude estimators was performed in a series of flight tests using a Beechcraft Queen Air test aircraft described in [15]. The aircraft was equipped with the following sensors.

1) A pair of low cost inertial measurement units (IMUs). The first IMU was the DMU-6X made by

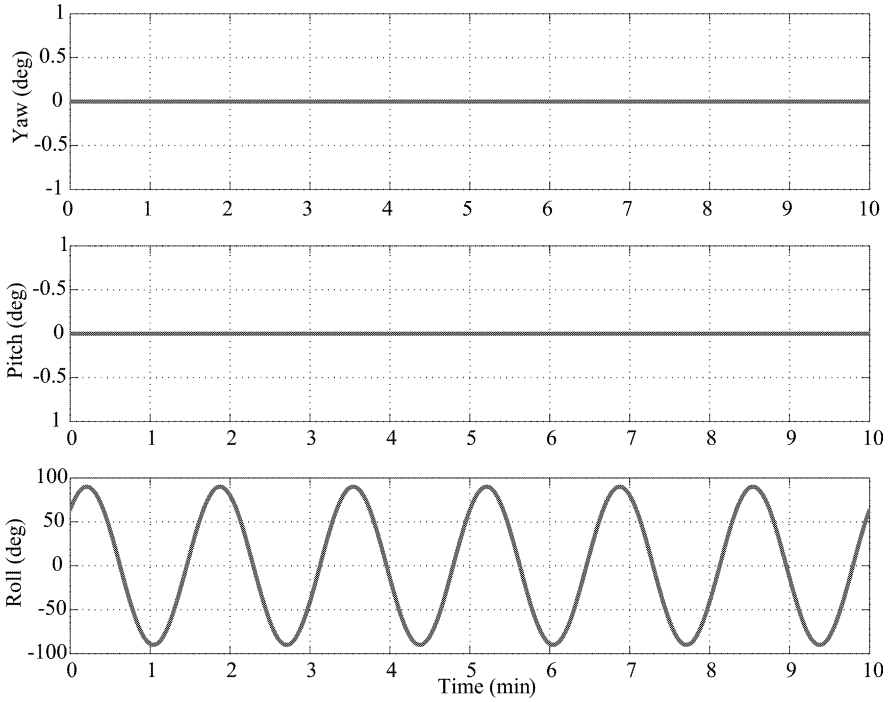

Fig. 15. Euler angle history. Large angular rates.

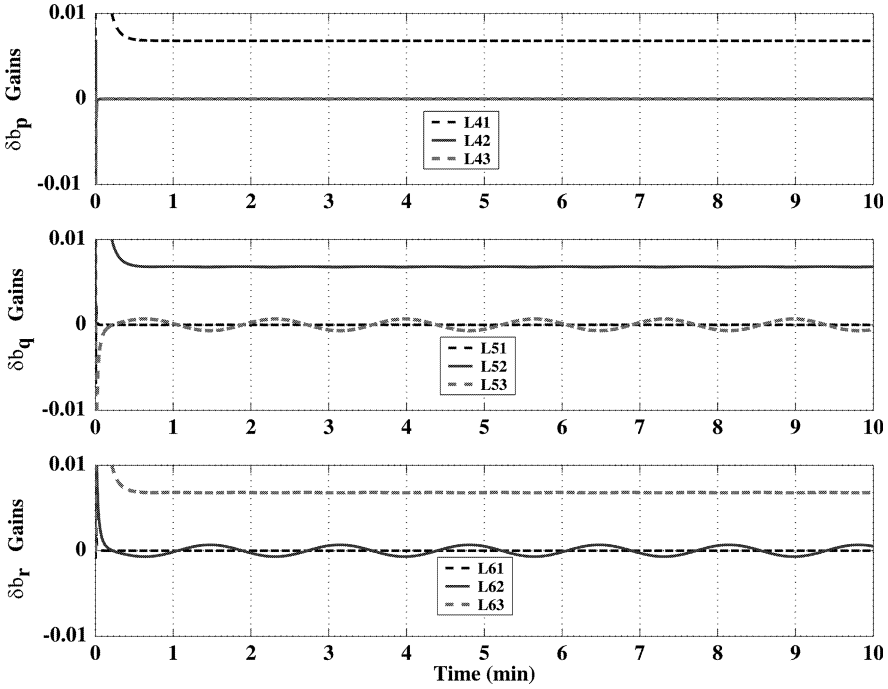

Fig. 16. Gain history for quaternion filter. Large angular rates.

Crossbow Technology. The second IMU was the DMU-AHRS all made by Crossbow. The sensor suite in these IMUs consisted of a triad of rate gyros and accelerometers. In addition, the DMU-ARHS had a magnetometer triad. The magnetometer triad in the DMU-AHRS was not used because its output was affected by interference from magnetic fields generated by the electronics in and around the IMU.

2) A low cost magnetometer triad (Honeywell HMR2300). The magnetometer triad was suitably located to avoid interference from unwanted magnetic fields generated by the aircraft's structure and avionics.

3) An orthogonally mounted triad of Systron-Donner "Horizon" rate gyros.

4) A navigation grade inertial reference unit (Honeywell YG1851 IRU). This system was used

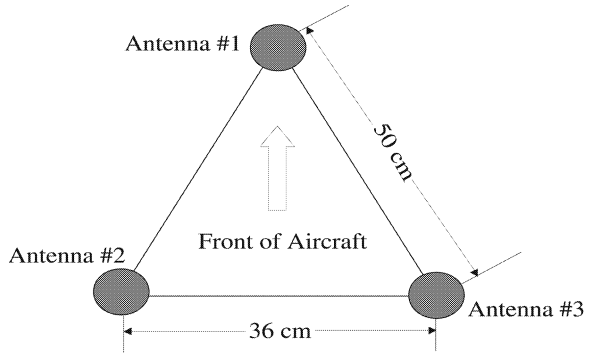

Fig. 17. Configuration of GPS antennas used with GPS attitude determination system.

to provide a highly accurate record of the aircraft's yaw, pitch, and roll angles. As such, it was used as a "truth" reference and the performance of the attitude estimators described here were compared with the outputs of this IRU.

5) A triple antenna short-baseline GPS attitude determination system. This system was used as one of the aiding systems. This system is described in [10] and uses three GPS antennas having the geometry shown in Fig. 17. The antenna triad was installed on the top of the aircraft's fuselage.

Performance of the Euler angle based estimator was verified in a real-time system that used Systron-Donner "Horizon" rate gyros aided by a multi-antenna GPS attitude determination system. The outputs from the three rate gyros were sampled at 20 Hz and numerically integrated to provide an estimate of the three Euler angles. The GPS attitude determination system generated Euler angle estimates at 2 Hz. The blending of the GPS and rate gyro attitude solution occurred at a 2 Hz rate. As noted earlier, to minimize the computational burden, the estimator used steady state Kalman gains. Table III lists the numerical values for the various parameters used in mechanizing this filter.

TABLE III
Summary of Numerical Values for Parameters in Euler Angle Filter

Matrix	Matrix Parameter	Numerical Values	Relevant Equation(s)
R_v	σ_ψ σ_θ σ_ϕ	0.25°	Equation (28)
Q_w (Wideband)	α	0.2	Equation (22)
	σ_p σ_q σ_r	0.05°/s	Equations (8) and (16)
Q_w (Correlated)	β	2.0×10^{-4}	Equation (22)
	σ_w	0.05°/s	Equations (8), (10) and (16)

Fig. 18 shows the real-time estimate of the gyro biases after filter start-up. It can be seen that the estimates of gyro biases stabilized after 3 to 4 min from power up. On-line estimation of the rate gyro biases allows the AHRS to coast during momentary GPS outages. To demonstrate this coasting capability, the estimator gain L was set to zero (in post process) to simulate an extended GPS outage. The plots in Fig. 19 show the deviation between the gyro integrated attitude solution and the GPS attitude solution during this simulated outage. At $t = 0$, the estimator gain is set to zero. There is less than a 4 deg error in all axes 5 min after the GPS feedback has been removed. Experience has shown that GPS outages in flight are rare and of a short duration lasting at most a few seconds. Fig. 19 clearly shows that the Systron Donner "Horizon" rate gyros can adequately coast through such short outages.

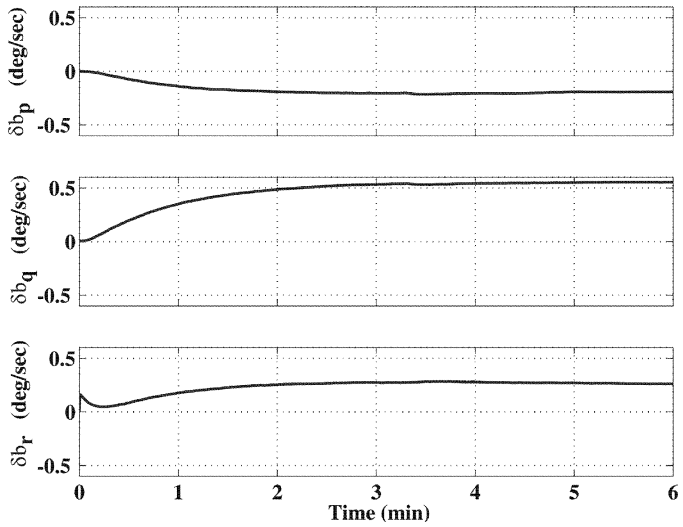

Fig. 18. Real-time estimation of biases for inexpensive rate gyros (Systron-Donner "Horizon" solid-state rate gyro).

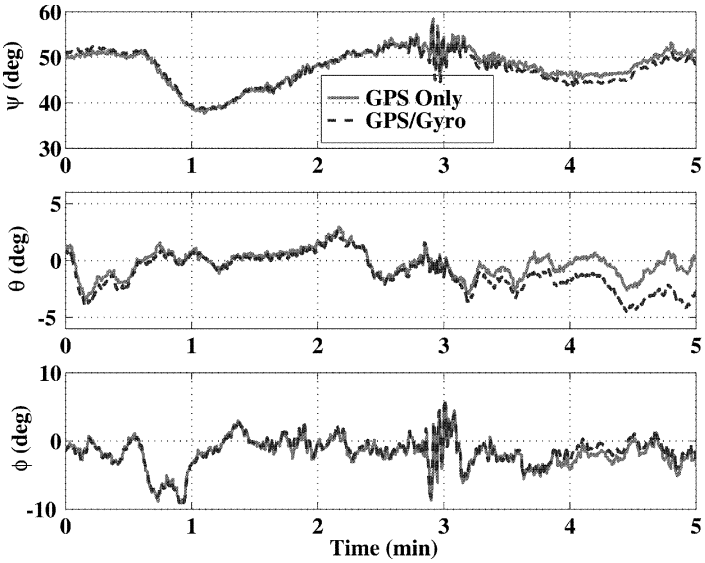

Fig. 19. Attitude time history and gyro coast capability (Systron-Donner "Horizon" solid-state rate gyro).

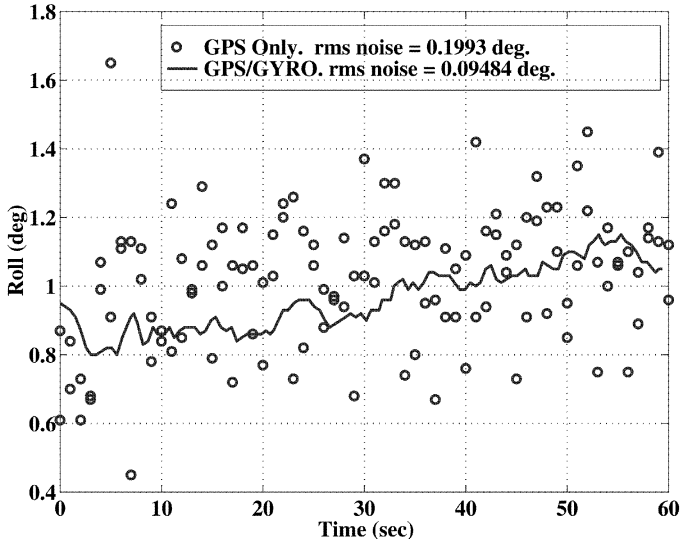

Fig. 20. Filtering of GPS attitude noise by inexpensive rate gyros (Systron-Donner "Horizon" solid-state rate gyro).

The attitude solution generated by this estimator was used to drive an advanced glass-cockpit display used by pilots for control of aircraft attitude. The display is discussed in [20] and [21]. This meant that the attitude solution generated had to have very little jitter and lag. This was achieved by selecting the appropriate values for the estimator tuning parameters α and β. A method of trial-and-error was used to select the values of the tuning parameters, α and β, defined in (22). Fig. 20, which is a close-up of the pitch solution generated by the real-time system, shows that the attitude solution is indeed jitter free. This demonstrates that the high-bandwidth information from the gyros has eliminated jitter in the attitude solution generated by the triple antenna GPS attitude system.

Performance of the quaternion-based estimator was verified in a system that used Crossbow DMU-6X and DMU-AHRS rate gyros aided by an accelerometer-magnetometer attitude system. In this aiding system, the accelerometers provided pitch and roll measurements while the magnetometers provided the yaw measurement. As noted earlier, the accelerometer-magnetometer aiding system does not provide an accurate attitude estimate when the aircraft is accelerating. When the magnitude of the acceleration is small and of a short duration, the effect of the acceleration is minimal. However, in prolonged accelerations (as would occur in turns), the blended attitude solution will diverge if the feedback from the accelerometers and magnetometer is used. This is the fundamental difference between this

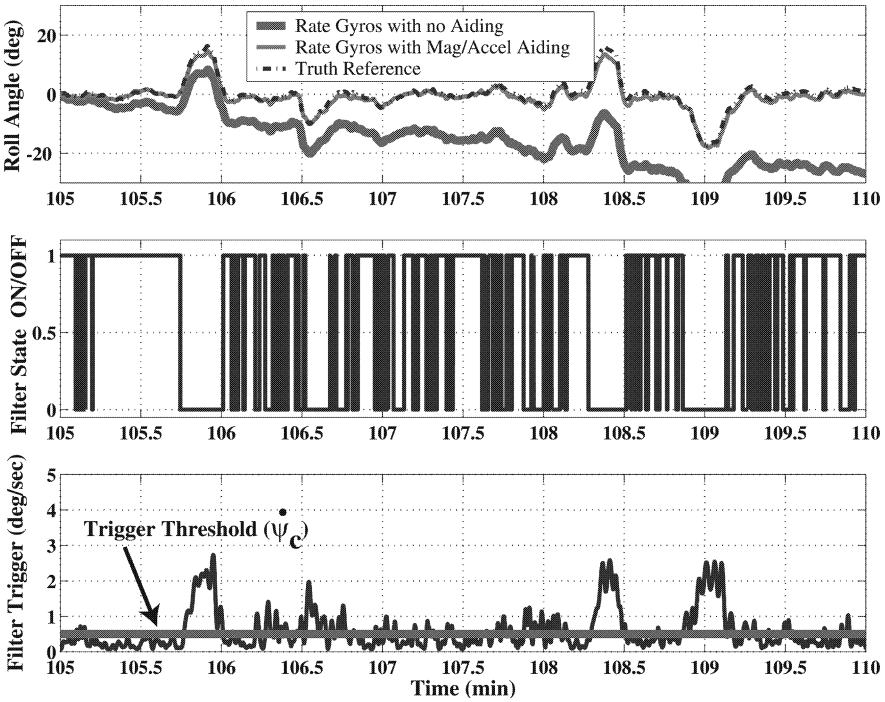

Fig. 21. Roll solution: DMU-6X gyros aided by accelerometer and magnetometer.

and the GPS aided system: with the accelerometer and magnetometer aiding system, the measurement updates must be turned off occasionally. This difference is shown schematically in Fig. 1 as a switch in the aiding system feedback path.

What trigger should be used to determine when to stop feedback from the aiding system? It was found that using a computed yaw rate, $\dot{\psi}_c$, works well as a trigger. That is, the computed yaw rate $\dot{\psi}_c$ defined as the difference between the yaw solution at the current time step, ψ_k, and the previous time step ψ_{k-1}, divided by the elapsed time Δt is used as the trigger to turn-on and off the aiding system feedback. Mathematically, this is given by

$$\dot{\psi}_c = \frac{\psi_k - \psi_{k-1}}{\Delta t}. \tag{51}$$

For a system that used the DMU-6X or DMU-AHRS rate gyros, it was found that a $\dot{\psi}_c$ threshold value of 0.5°/s performed satisfactorily. Whenever the value of $\dot{\psi}_c$ exceeded 0.5°/s, the filter assumed the vehicle was in a turn and hence, accelerometer feedback was turned off. In addition, for the cases where the acceleration is not induced by turning, the magnitude of the accelerometer specific force measurement is checked. If it is less than a certain threshold, the feedback is kept on. The threshold was set to $1.05g$ for the AHRS discussed in this paper. That is, if the magnitude of the accelerometer readings is in excess of $1.05g$, then feedback from the accelerometers is turned off.

It is conceivable that during the sustained acceleration of a constant speed turn, the pitch attitude errors can be kept small by using the f_x accelerometer output (see (18)). This is because in a coordinated, constant speed turn, f_x will not be affected by centripetal acceleration. The f_y accelerometer, however, is affected by centripetal accelerations and cannot be used to keep roll errors bounded. Thus, unless another measurement from a device such as an air speed sensor is incorporated, it is particularly difficult to keep the roll errors small during long duration turns.

Experimental flight test results verifying performance of the quaternion-based filter are shown in Fig. 21. The results shown are for the system that used the DMU-AHRS rate gyros. The performance of the rate gyros in the DMU-AHRS IMU is slightly better than those in the DMU-6X but significantly worse than the fiber optic gyros for which error models were given in Table I. Therefore, for simplicity, the attitude filter was mechanized using error model parameters for the DMU-6X rate gyros. The numerical values listed in Table IV were used to compute the steady state gains off-line. Note that the measurement noise on pitch and roll were obtained by converting the accelerometer and magnetometer wideband noise into an angular measurement using (18), (19), and (20). In Fig. 21, we only show the roll solution because the performance of this estimator is similar to the GPS aided estimator with the major difference being the aiding system feedback switch. Operation of this switch is most apparent during maneuvers that involve changes in roll attitude. The top-most plot in the figure shows a comparison of the attitude solution from a navigation grade IRU,

TABLE IV
Numerical Values for Filter Parameters in Accelerometer/Magnetometer AHRS

Matrix	Matrix Parameter	Numerical Values	Relevant Equation(s)
R_v	σ_ψ	0.80°	Equation (20)
	σ_θ σ_ϕ	0.06°	Equation (18) Equation (19) and (28)
Q_w (Wideband)	α	10	Equation 39
	σ_p σ_q σ_r	0.05°/s	Equations (8) and (16)
Q_w (Correlated)	β	1.0×10^{-5}	Equation 39
	σ_w	0.05°/s	Equations (8), (10) and (16)

a low-performance solid-state gyro aided by an accelerometer and magnetometer and open-loop integration of the same gyro. As noted earlier, the attitude solution from the navigation grade IRU is used as a truth reference. The open-loop solution is seen to diverge. This is not surprising because the output bias instability and wideband noise for these low-performance gyros can be large. As would be expected, the attitude errors when the system is aided by accelerometers and magnetometers is bounded. The second plot in Fig. 21 shows the filter state. The filter state indicates whether the accelerometer and magnetometer feedback switch is on or off. The last plot shows the computed yaw rate that is used to trigger the filter on or off. What is clear from these three plots is that the filter turns itself off when in turns.

Accelerations where the aircraft is not turning are of very limited duration. The long accelerations occur in turns. Thus, if turns are limited to short duration this aiding scheme will work acceptably. However, if turns are of a long duration, the gyros will be integrated open-loop and the attitude solution will drift.

X. CONCLUSIONS

This paper described the mechanization of AHRS that relied on low-performance rate gyros. The basic idea behind the mechanization techniques described was the idea of complementary filtering. That is, rate gyros are combined with an aiding system. Normally, the aiding system selected should have an output error that does not have a bias but may be corrupted by wideband noise. Thus the fusion of the rate gyros with the aiding system results in a blended output that has high bandwidth (due to the gyros) and errors that are wideband in nature (due to the aiding system). While there are many ways to parameterize the attitude (and, thus, the estimator), only Euler angle and quaternion mechanizations were discussed. Quaternion implementation of the sensor fusion algorithms have several advantages. Notably, gain scheduling is easier and more efficient when quaternions are used. In addition, the time update equation for the quaternion filter does not involve transcendental functions and, thus, is computationally easier to implement on inexpensive microprocessors with limited processing power.

The aiding systems discussed were mechanized using multiple GPS antennas, magnetometers, and accelerometers. The magnetometer and accelerometer aiding system had a limitation in that its attitude information could not be relied on during maneuvers that involved significant accelerations. This limitation can be mitigated by incorporating acceleration information derived from an air speed sensor or GPS. Such an aiding system is discussed in [7]. In closing we note that such AHRS are beginning to appear in general aviation aircraft. Furthermore, they and have the potential of being an important subsystem of a dead reckoning navigator which can be used as a backup to GPS [15].

ACKNOWLEDGMENTS

We thank the management and test pilots of Sky Research Inc., for providing high quality and safe flight testing services. We also gratefully acknowledge the support of many of our colleagues in the Stanford University GPS Laboratory.

REFERENCES

[1] Goodrich Sensor Systems (2000)
Specification Sheet for VG34 Vertical Gyro.
Goodrich Corporation, Burnsville, MN, 2000.

[2] Systron Donner Inertial Division (1998)
Specification Sheet for BEI Gyrochip Model "HORIZON" Micromachined Angular Rate Sensor.
BEI Technology, Inc., Concord, CA, 1998.

[3] Silicon Sensing Systems (2000)
Specification Sheet for CRS03 Silcon Rate Sensor.
Silicon Sensing Systems Ltd., Plymouth, England, 2000.

[4] KVH Fiber Optic Group (2001)
Specification Sheet for KVH E-Core 1000 Fiber Optic Gyro.
KVH Industries, Inc., Tinley Park, IL, 2001.

[5] Honeywell Military Avionics Group (1997)
Specification Sheet for HG1700 Inertial Measurement Unit.
Honeywell, Inc., Minneapolis, MN, 1997.

[6] Kornfeld, R. P., Hansman, R. J., and Dyest, J. J. (1998)
Single antenna GPS based attitude determination.
In *Proceedings of the Institute of Navigation National Technical Meeting ION-NTM*, Long Beach CA, Jan. 1998.

[7] Gebre-Egziabher, D., Elkaim, G. H., Powell, J. D., and Parkinson, B. W. (2000)
A gyro-free, quaternion based attitude determination system suitable for implementation using low-cost sensors.
In *Proceedings of the IEEE Position Location and Navigation Symposium* (PLANS 2000), 185–192.

[8] Wahba, G. (1966)
Problem 65-1 (solution).
SIAM, Review, **8** (1966), 384–386.

[9] Cohen, C. E. (1992)
Attitude determination using GPS.
Ph.D. dissertation, Stanford University, Stanford, CA, Dec. 1992.

[10] Gebre-Egziabher, D., Hayward, R. C., and Powell, J. D. (1998)
A low cost GPS/inertial attitude heading reference system (AHRS) for general aviation applications.
In *Proceedings of the IEEE Position Location and Navigation Symposium* (PLANS 1998), 518–525.

[11] Creamer, G. (1996)
Spacecraft attitude determination using gyros and quaternion measurements. *The Journal of Astronautical Sciences*, **44**, 3 (July–Sept. 1996), 357–371.

[12] Thompson, I. C., and Quasius, G. R. (1980)
Attitude determination for the P80-1 satellite.
Presented at the AAS Guidance and Control Conference, Keystone, CO, Feb. 1980, AIAA Paper 80-001.

[13] Lefferts, E. J., Markley, F. L., and Shuster, M. D. (1982)
Kalman Filtering for spacecraft attitude estimation.
AIAA Journal of Guidance Control and Navigation, **5**, 5 (Sept.–Oct. 1982), 417–429.

[14] Kuipers, J. B. (1999)
Quaternions and Rotation Sequences.
Princeton, NJ, Princeton University Press, 1999.

[15] Gebre-Egziabher, D. (2001)
Design and performance analysis of a low-cost aided-dead reckoning navigation system.
Ph.D. dissertation, Department of Aeronautics and Astronautics, Stanford University, Stanford, CA, Dec. 2001.

[16] Friedland, B. (1986)
Control System Design: An Introduction to State Space Methods.
New York: McGraw-Hill, 1986.

[17] Franklin, G. F., Powell, J. D., and Workman, M. L. (1994)
Digital Control of Dynamic Systems.
Menlo Park, CA: Addison Wesley, 1994.

[18] Hayward, R. C., Gebre-Egziabher, D., Schwall, M., Powell, J. D., and Wilson, J. (1997)
Inertially aided GPS based attitude heading reference system (AHRS) for general aviation aircraft.
In *Proceedings of the Institute of Navigation ION-GPS Conference*, 1997, 1415–1424.

[19] Stengel, R. F. (1994)
Optimal Control and Estimation.
New York: Dover, 1994, 299–419.

[20] Barrows, A. K., Gebre-Egziabher, D., Hayward, R. C., Xia, R., and Powell, J. D. (1996)
GPS-based attitude and guidance displays for general aviation.
In *Proceedings of the IEEE Emerging Technologies and Factory Automation Symposium*, Kauai, HI, 1996.

[21] Barrows, A. K. (2000)
GPS 3-D cockpit displays: Sensors, algorithms, and flight testing.
Ph.D. dissertation, Department of Aernautics and Astronautics, Stanford University, Stanford, CA, May 2000.

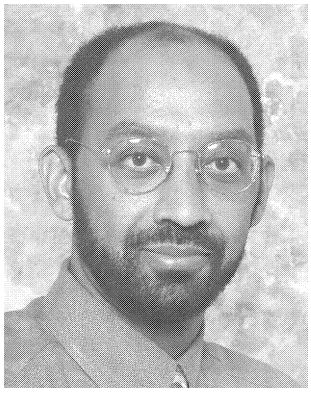

Demoz Gebre-Egziabher received a B.S. in aerospace engineering from the University of Arizona, Tuscon, in 1990, an M.S. in mechanical engineering from the George Washington University, Washington, D.C., in 1996, and a Ph.D. in aeronautics and astronautics from Stanford University, Stanford, CA, in 2002.

He is currently an assistant professor of Aerospace Engineering and Mechanics at the University of Minnesota, Twin Cities Campus. His research focuses on the development of robust GPS based navigation systems and the design of multi-sensor navigation, guidance, and attitude determination systems for aerospace and ground vehicles.

Roger C. Hayward received an S.B. degree in aeronautics and astronautics from MIT, Cambridge, MA, and an M.S. in aeronautics and astronautics from Stanford University, Stanford, CA.

Currently, he is president of GeoTrax Protection LLC. His research interests include GPS based attitude determination and the design of low cost navigation and positioning systems.

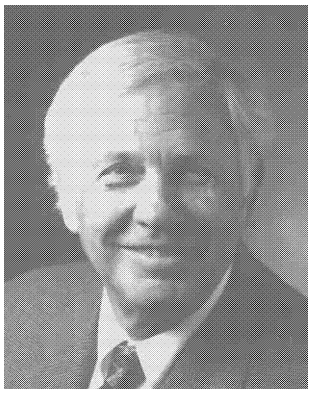

J. David Powell received his B.S. degree in mechanical engineering from MIT, Cambridge, MA, in 1960 and his Ph.D in aeronautics and astronautics from Stanford University, Stanford, CA, in 1970.

He joined the Stanford Aeronautics and Astronautics Department and the Mechanical Engineering Department Faculty in 1971 and is currently an emeritus professor. Recent focus of research is the use of GPS-based attitude determination augmented with inertial sensors, applications of the FAA's WAAS for enhanced pilot displays, and the use of WAAS and new displays to enable closer spacing on parallel runways.

Dr. Powell has coauthored two text books in control systems design.